

## AlMn Transition Edge Sensors for Advanced ACTPol

Dale Li<sup>1,2</sup> · Jason E. Austermann<sup>2</sup> · James A. Beall<sup>2</sup> · Daniel T. Becker<sup>2</sup> · Shannon M. Duff<sup>2</sup> · Patricio A. Gallardo<sup>3</sup> · Shawn W. Henderson<sup>3</sup> · Gene C. Hilton<sup>2</sup> · Shuay-Pwu Ho<sup>4</sup> · Johannes Hubmayr<sup>2</sup> · Brian J. Koopman<sup>3</sup> · Jeffrey J. McMahon<sup>5</sup> · Federico Nati<sup>6</sup> · Michael D. Niemack<sup>3</sup> · Christine G. Pappas<sup>4</sup> · Maria Salatino<sup>4</sup> · Benjamin L. Schmitt<sup>6</sup> · Sara M. Simon<sup>4</sup> · Suzanne T. Staggs<sup>4</sup> · Jeff Van Lanen<sup>2</sup> · Jonathan T. Ward<sup>6</sup> · Edward J. Wollack<sup>7</sup>

Received: 1 October 2015 / Accepted: 22 January 2016 / Published online: 17 February 2016  
© Springer Science+Business Media New York 2016

**Abstract** Advanced ACTPol (AdvACT) will use an array of multichroic polarization-sensitive AlMn transition edge sensor (TES) bolometers read out through time-division multiplexing. Aluminum doped with a low concentration of manganese can be deposited to a bulk film thickness for a more reliable superconducting critical temperature uniformity compared to thin bilayers. To build the TES, the AlMn alloy is deposited, over Nb wiring, to a specific thickness to set the TES normal resistance. The doping concentration of manganese coarsely defines the TES critical temperature, while a fine tuning is achieved by heating the deposited film to a specific temperature. The TES island is connected to the thermal bath via four silicon-nitride membranes, where their geometry defines the thermal conductance to the temperature of the bath. Lastly, the TES heat capacity is increased by addition of PdAu electrically connected to the AlMn film. Designs and performance characteristics of these AlMn TESs are presented for use in AdvACT.

**Keywords** Transition edge sensor · AlMn · Bolometer · Thin film · Superconductor · Microfabrication · Heating · Critical temperature

---

✉ Dale Li  
dale.li@slac.stanford.edu

<sup>1</sup> SLAC National Accelerator Laboratory, 2575, Sand Hill Road, Menlo Park, CA 94025, USA

<sup>2</sup> National Institute of Standards and Technology, 325 Broadway, Boulder, CO 80305, USA

<sup>3</sup> Department of Physics, Cornell University, Ithaca, NY 14853, USA

<sup>4</sup> Department of Physics, Princeton University, Princeton, NJ 08544, USA

<sup>5</sup> Department of Physics, University of Michigan, Ann Arbor, MI 48103, USA

<sup>6</sup> Department of Physics and Astronomy, University of Pennsylvania, Philadelphia, PA 19104, USA

<sup>7</sup> NASA Goddard Space Flight Center, Greenbelt, MD 20771, USA

## 1 Introduction

Advanced ACTPol (AdvACT) is the third-generation cosmic microwave background (CMB) telescope for the Atacama Cosmology Telescope (ACT) project in the Atacama Desert, Chile [1]. This upgrade includes independent arrays of feedhorn-coupled polarization-sensitive detectors with transition edge sensors each housed in a separate optics tube in a common dewar at dilution refrigerator temperatures. A total of five frequency bands are sampled in multichroic sensitive pixels: 28/41 GHz, 90/150 GHz, and 150/230 GHz. The low-frequency 28/41 GHz array will be made of large single pixels. The mid-frequency 90/150 GHz array is an improvement to the current ACTPol PA3 array also sensitive to 90/150 GHz, which is currently being used for observations of the sky [2,3]. The high-frequency 150/230 GHz array is scaled from the mid-frequency array. Improvements for AdvACT include monolithic fabrication on 150-mm wafers instead of using six sub-arrays fabricated on 3-inch wafers as was the case for the second-generation project, ACTPol [4]. Additionally, silicon-nitride insulators were developed to replace silicon-oxide dielectrics in order to improve the loss tangent and thus the optical efficiency of the devices. Further details of these fabrication developments can be found elsewhere [5].

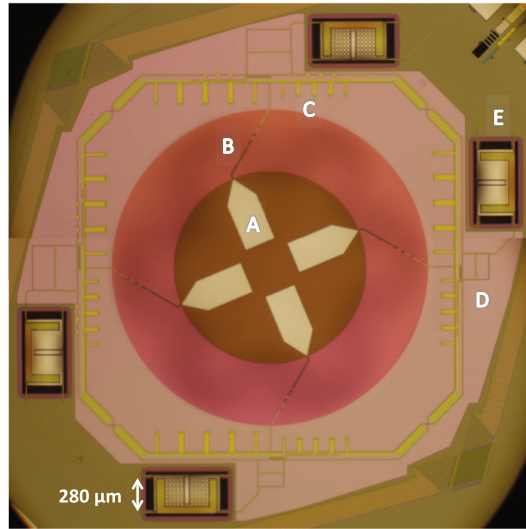
In this paper, we describe the transition edge sensor (TES) that was specifically designed for AdvACT. Doping aluminum films with manganese to tune the critical temperature has been described elsewhere [6–8], and implemented successfully for the South Pole Telescope in its current deployment [9–11]. The ACTPol detectors utilized TESs made from molybdenum–copper bilayers [12]. Several challenges were associated with upgrading the ACTPol designs from monolithically fabricated 3-inch-diameter arrays to monolithically fabricated 150-mm-diameter arrays for AdvACT including uniformity and precision in the TES critical temperature, interlayer adhesion, and etch uniformity [5]. Switching from a bilayer TES to a single deposited layer of an aluminum alloy tuned with a specific concentration of manganese simplified or avoided many of the challenges associated with scaling to larger arrays.

## 2 Advanced ACTPol Pixel Design

Figure 1 shows an optical micrograph of a prototype test pixel for the high-frequency 150/230 GHz design. There are four TES islands, each associated with a different frequency band and polarization combination. In this compact design, each pixel including the associated array-level wiring can be arranged in a hexagonal close-packed lattice with a nearest-neighbor spacing of 4.75 mm. The mid-frequency pixels at 90/150 GHz will have a wider spacing of 5.3 mm, while the low-frequency pixels will be designed as individual pixels arranged in a grid.

Many fabrication improvements were implemented for AdvACT building upon the successful deployment of the second-generation telescope ACTPol, now currently on the sky in Chile [2,3]. ACTPol deployed a first of its kind array of multichroic pixels at 90 GHz and 150 GHz pieced together from six sub-arrays each monolithically fabricated from 3-inch wafers. For AdvACT, much effort was made to move to a single fabricated 150-mm wafer, which required significant improvements to both deposition

**Fig. 1** A single multichroic pixel for the 150/230 GHz high-frequency array in AdvACT. Light from the CMB enters a micro-machined feedhorn [13] and excites Nb fins (*a*), then travels along a Nb coplanar waveguide, and transitions to a Nb microstrip (*b*); band-defining stub filters (*c*) pick out a frequency window (in this case around 230 GHz); signal from two opposing fins enters a microwave hybrid-tee (*d*) where the sum port is dissipated to the silicon substrate via a gold meandering strip, while the difference port is dissipated onto a TES island (*e*) (Color figure online)



and etch uniformity over a larger area, improvements in dielectric materials, and an overhaul of the wiring patterns for a more systematic approach to array-level wiring for readout [5].

### 3 Advanced ACTPol TES Design

Another significant change from ACTPol to AdvACT is the TES material. In ACTPol, a bilayer of molybdenum and copper was used to tune a critical temperature,  $T_c$ , based on the layer thicknesses and their mutual proximity effects. At dilution refrigerator temperatures, a target TES  $T_c$  of 160 mK requires a very thin Mo layer ( $\sim 60$  nm). At this thickness, small variations in deposition rates from run to run can have a significant impact on the  $T_c$ , which then affects the detector sensitivity. In addition, adhesion to copper surfaces becomes increasingly problematic for fabrication processes with alternating layers of insulator and metal.

In the effort to improve repeatability, uniformity, and adhesion, we redesigned the TES to eliminate the bilayer and replace it with an alloy of aluminum doped with manganese. An additional benefit to this design change eliminates the need for a copper bank to proximitize the edge of the bilayer, as is required with MoCu (or any other bilayer). Because AlMn is an alloy, it is sputter-deposited in one step, greatly simplifying the TES deposition process. Furthermore, the normal resistance for an AlMn film can be set by the film thickness and can be decoupled from the  $T_c$  in the bulk film limit. For AdvACT, we were able to achieve a uniform  $T_c$  within 1 % over a 150-mm wafer without the need for a highly uniform thickness.

Figure 2 shows the TES design for AdvACT. We tested different geometries for the different components of the TES island in order to optimize the performance of the TES for AdvACT [15]. For example, different AlMn aspect ratios were achieved

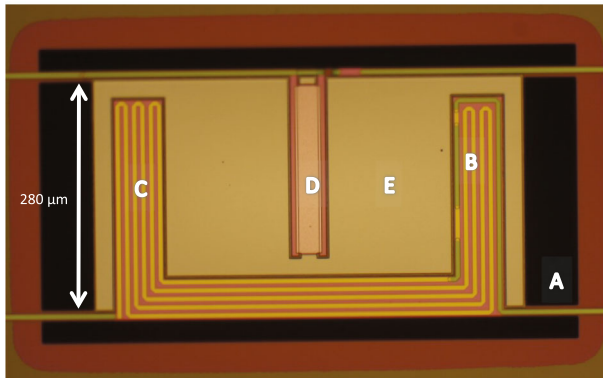


**Fig. 2** Close-up view of an AlMn TES bolometer for AdvACT. Silicon-nitride legs define the thermal conductance of the island to the silicon substrate. The sum port from the hybrid-tee connects to the microstrip trace on one of the legs (*a*) and transitions to a meandering gold trace (*b*). Through the length of the gold meander (*c*), energy is dissipated onto the island in the form of heat. A thin film of aluminum doped with a low concentration of manganese (2000 ppm by atomic %) is at (*d*). The island's total heat capacity can be modified by changing the thickness of a normal metal of PdAu (*e*) (Color figure online)

simply by changing the distance between the leads in Fig. 2d, which adjusts the normal resistance by changing the number of squares between the Nb leads. Another adjusted parameter was the silicon-nitride leg widths. These adjustments predictably changed the thermal conductance linearly with leg width giving a well-controlled knob to tune the saturation power [15]. Also adjusted was the PdAu thickness and area, which predictably controlled the time constant by changing the heat capacity of the island.

#### 4 Heat Treatment for AlMn Films

The most important aspect of the TES that was adjusted was the TES material itself. Aluminum doped with manganese in different amounts had previously been shown to predictably control the  $T_c$  of superconducting films [6–8]. However, the  $T_c$  can also be highly sensitive to film thickness especially in the thin-film regime. We also observed a change in  $T_c$  due to heating, which would be devastating for any microfabrication process requiring the baking of photoresist for lithography.

Fortunately, the heating process actually provided a much more reliable way to achieve reproducible  $T_c$  than either fine tuning the thickness, or attempting to adjust the manganese concentration. Although the manganese concentration does broadly set the  $T_c$ , frequently changing a sputtering target or trying to find a manufacturer to adjust the manganese concentration by tens of ppm is impractical. Figure 3 plots the measured  $T_c$  of films as a function of bake temperature. In this plot, five different wafers were sputtered each with different thicknesses of aluminum doped with 2000 ppm of manganese by atomic percentage. Each of these wafers were subsequently diced and the chips were heated to different temperatures on a hot plate for 10 min each. A cluster of points near 180 °C shows chips that were first heated to 180 °C and then heated for a second time to lower temperatures. The small variation in  $T_c$  of these points suggest

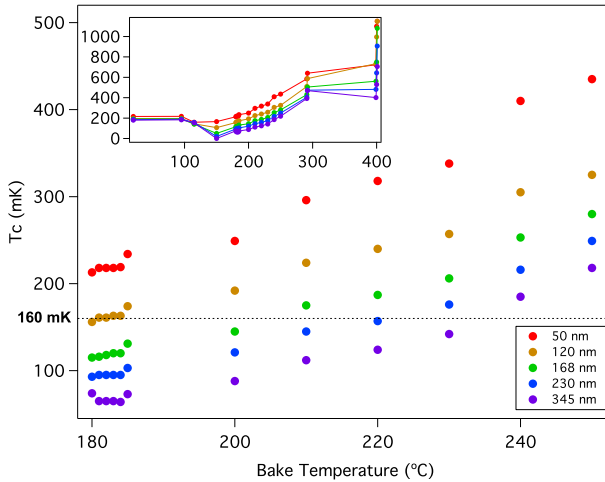


**Fig. 3** Heat setting the critical temperature,  $T_c$ , of AlMn by baking. Aluminum doped with 2000 ppm manganese is deposited by sputtering on five different wafers with different thicknesses (see legend at lower right). Each of these wafers are diced into pieces and each subsequent piece is heated on a hot plate to a different temperature for 10 min.  $T_c$  was measured cryogenically in an adiabatic demagnetization refrigerator. Many trials at 180 °C indicate samples that were initially heated at 180 °C and then subsequently heated at lower temperatures in order to test  $T_c$  drift in processing. The inset shows the full range of  $T_c$ , with an initial dip and then climb to near the  $T_c$  of pure aluminum (Color figure online)

that additional heating of the AlMn films does not significantly affect the  $T_c$ , as long as the initial bake temperature was higher.

Baking of the AlMn films not only yields a reproducible and predictable  $T_c$  but also protects the film from changes in  $T_c$  due to the typical heating during a fabrication process. Lithographic steps can regularly heat the films up to 150 °C. It is interesting to note that in the inset of Fig. 3, the aluminum  $T_c$  is nearly recovered once the films are heated to a high enough temperature, albeit with an increasingly larger spread. The mechanism of how the  $T_c$  changes due to heating is still unknown. While AlMn has a complicated phase diagram [16], with even more complicated structural formations [17], it is surprising that such relatively low baking temperatures can appreciably affect the  $T_c$  without greatly affecting the normal state resistance, though some small changes were observed.

Nevertheless, using the baking prescription from Fig. 3 with films of thickness 400 nm, we were able to achieve a low normal resistance (4–8 m $\Omega$ ), which is required for time-domain multiplexing in AdvACT, with a well-controlled target  $T_c$  with a uniformity of 1% over a 150-mm wafer. In this way, we achieved a uniform  $T_c$  without the need for a highly uniform film thickness. Some additional data with different manganese concentrations indicate qualitatively similar sensitivity to bake temperature, though more research is needed. It is worth noting that for these detector applications, a small spread in the normal resistance is tolerable compared to a spread in  $T_c$ , which would affect the saturation powers and therefore the ability to uniformly bias the array.

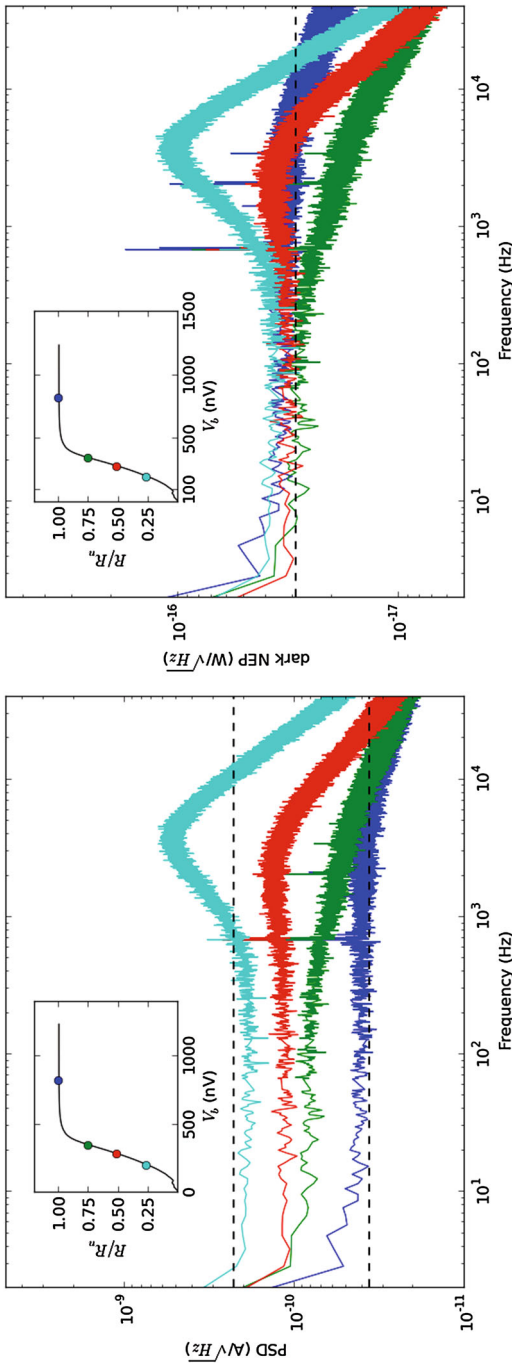


**Fig. 4** The left plot is the TES current noise in power spectral density (PSD) measured in  $A/\sqrt{Hz}$  versus frequency. The upper dashed line is the white noise expectation from a superconductor, while the lower dashed line is the noise expected from the normal resistance. The right plot is the TES noise equivalent power (NEP) measured in  $W/\sqrt{Hz}$  versus frequency. Here, the dashed line refers to the expected noise due to the thermal conductance of the silicon-nitride legs. Both figures include an inset showing the bias point for each colored plot. 60 Hz pickup noise and their harmonics were removed for clarity. Note that the NEP calibration should be a good estimate below 100 Hz but is not accurate at higher frequencies (Color figure online)

## 5 Performance Data for AlMn TES

Figure 4 shows the noise performance for an AlMn TES fabricated following the above bake prescription. Fig. 4 (left) is the power spectral density as a function of frequency for four different bias points of the TES (as indicated in the inset). Because the TES behavior largely remains between the white noise set in the superconducting phase and the white noise set in the normal resistive phase throughout the transition, we can conclude that the TES is well behaved and stable. Fig. 4 (right) is the noise equivalent power (NEP) as a function of frequency derived from the current noise with the dc responsivity. Even at different bias points, the NEP follows the predicted noise from considering the thermal conductance of the silicon-nitride legs and the AlMn  $T_c$ . These noise measurements were performed on TES islands without the addition of PdAu to adjust the heat capacity. Low-frequency noise measurements could be improved in the future with more stable bath temperatures or cross correlation between multiple devices. It should be noted that the NEP calibration assumes a scaling of the DC responsivity from the IV curve (insets) and is only a good estimate for frequencies below 100 Hz.

## 6 Conclusions

Alloys of aluminum doped with manganese can be sputter-deposited at a thickness that defines the normal state resistance, while the  $T_c$  can be dialed coarsely by manganese concentration, and finely by baking the film in a controlled manner. This initial bake temperature should be higher than all subsequent heating of the film to ensure that the  $T_c$  will not change further during fabrication. A  $T_c$  uniformity within 1 % over a 150-mm wafer can be achieved in this method without requiring the same uniformity in thickness. These AlMn TES designs have been shown to exhibit well-behaved noise performance, and are compatible with existing fabrication steps for the production of science- grade polarimeter arrays for AdvACT. The next generation of CMB telescopes, CMB Stage-4, will require a significant increase in pixel density scaling. Improvements in fabrication techniques, materials, yield, and uniformity control such as these implemented for AdvACT will push CMB science forward into the next frontier.

**Acknowledgments** This work was supported by the U.S. National Science Foundation through awards 1312380 and 1440226. The NIST authors would like to acknowledge the support of the NIST Quantum Initiative. The development of multichroic detectors and lenses was supported by NASA Grants NNX13AE56G and NNX14AB58G. The work of BJK, BLS, JTW, and SMS was supported by NASA Space Technology Research Fellowship awards.

## References

1. S. W. Henderson et al., J. Low Temp. Phys. LTD16. (this Special Issue)
2. R. Datta et al., J. Low Temp. Phys. LTD16. (this Special Issue)
3. S. -P. Ho et al., J. Low Temp. Phys., in this Special Issue
4. M.D. Niemack et al., Proc. SPIE **7741**, 77411S (2010)
5. S. M. Duff et al., J. Low Temp. Phys., in this Special Issue

6. G. Boato et al., Phys. Rev. **148**, 353 (1966)
7. G. O'Neil et al., J. Appl. Phys. **107**, 093903 (2010)
8. B.A. Young et al., Accelerators, spectrometers, detectors and associated equipment. Nucl. Instrum. Methods Phys. Res. Sect. A **520**(1), 307 (2004)
9. E. M. George et al., in *Proceedings of the SPIE 8452*, Millimeter, Submillimeter, and Far-Infrared Detectors and Instrumentation for Astronomy VI, 84521F (2012); doi:[10.1117/12.925586](https://doi.org/10.1117/12.925586)
10. E.M. George et al., J. Low Temp. Phys. **176**(3), 383 (2014)
11. J. E. Ausermann et al., in *Proceedings of the SPIE 8452*, Millimeter, Submillimeter, and Far-Infrared Detectors and Instrumentation for Astronomy VI, 84521E (2012); doi:[10.1117/12.927286](https://doi.org/10.1117/12.927286)
12. E.A. Grace et al., IEEE Trans. Appl. Supercond. **23**(3), 2500704 (2013)
13. S. Simon et al., J. Low Temp. Phys. LTD16. doi:[10.1007/s10909-015-1370-2](https://doi.org/10.1007/s10909-015-1370-2) (this Special Issue)
14. K.D. Irwin, G.C. Hilton, in *Transition-Edge Sensors*. Cryogenic Particle Detection, (Springer, New York, 2005), pp. 63–150
15. K. T. Crowley et al., in *Proceedings of the 36th ESA Antenna Workshop*, 2015
16. P.D. Desai, J. Phys. Chem. Ref. Data **16**(1), 109 (1987)
17. D. Shechtman et al., Phys. Rev. Lett. **53**(20), 1951 (1984)